Supplementary Information

Theory of Shaping Electron Wavepackets with Light

Ori Reinhardt and Ido Kaminer[*]

Department of Electrical Engineering and Solid State Institute, Technion, Israel Institute of Technology, 32000 Haifa, Israel

[*]Corresponding author e-mail: kaminer@technion.ac.il

Number of pages: 6

Number of figures: 3

S1. Error analysis for shaping electron wavepackets with light

In order to show the stability of the laser-driven electron wavepacket shaping, and of the shaper pulse found through our optimization algorithm, we present an error analysis for the case of shaping electron energy shift (Fig.2 of the main text). In Fig.S1 we focus on a specific choice of an energy shift from Fig.2 of the main text, and plot the electron spectra obtained from interacting with the optimal shaper pulse under the influence of random noise. We conclude that it is possible to achieve a stable electron energy shift even when using laser fields that deviate from the set of optimized values.
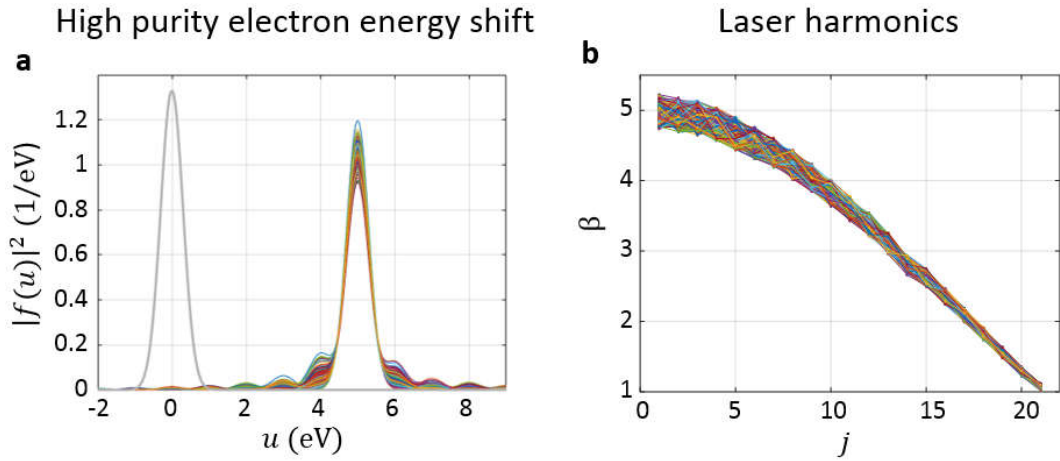
Figure S1: Robustness to errors in electron temporal shaping. (a) Electron energy spectrum after the interaction with random laser fields close to optimized values. The initial wavefunction is colored in gray. We use 21 laser harmonics to achieve a target energy shift of $5\hbar\omega$. (b) The noisy amplitudes of the shaper harmonics, corresponding to the plots in (a). The plot is constructed from 150 random realizations with a uniform random noise varying the amplitude $|\beta|$ by $\pm5\%$ and the phase $\arg(\beta)$ by ±0.05 rad.

S2. Theory of quantum electron interaction with arbitrary (continuous) laser spectra

Our analytical theory involves solving a Schrödinger equation for the free electron in the presence of a strong EM field that we consider as a classical time dependent potential. The Schrödinger equation is solved in the paraxial regime with corrections accounting for the relativistic nature of the electron. Here, we present the derivation of PINEM for the most general case of a field with an arbitrary spectrum $\vec{E}(\omega)$ at some frequency range. In this case the interaction Hamiltonian can be written as

$$H_1 = -\frac{e\hbar}{2m}\int_0^\infty d\omega \frac{1}{\omega}\left(e^{-i\omega t}\vec{E}_0(\omega)\cdot\vec{\nabla} - e^{i\omega t}\vec{E}_0^{\,*}(\omega)\cdot\vec{\nabla}\right). \tag{S1}$$

We apply an ansatz, writing the wavefunction of the electron during the interaction as

$\psi(\vec{r},t) = e^{i\left(k_0 z - \frac{U_0}{\hbar}t\right)}\tilde{\psi}(\vec{r},t)$, and after applying the PINEM approximations[68] we find the

equation for $\tilde{\psi}$ to be:

$$-\frac{ev}{2\hbar}\int_{-\infty}^\infty d\omega \frac{1}{\omega}\left(e^{-i\omega t}E_z(\omega) - e^{i\omega t}E_z^*(\omega)\right)\tilde{\psi} = v\frac{\partial\tilde{\psi}}{\partial z} + \frac{\partial\tilde{\psi}}{\partial t}, \tag{S2}$$

which can be decomposed into its spectrum $f(\omega,\vec{r})$ defined by

$$\tilde{\psi}(\vec{r},t) = S(\vec{r} - vt\hat{z})\int_{-\infty}^\infty f(\omega,\vec{r})e^{i\omega\left(\frac{z}{v}-t\right)}d\omega. \tag{S3}$$

with S an envelope function, representing the coherent profile of the initial electron pulse, e.g,
a Gaussian.

Solving for $f(\omega,\vec{r})$, under the assumption that $S(\vec{r} - vt\hat{z})$ is very wide, we can understand

$\left|f(\omega,\vec{r})\right|^2$ as the frequency-dependence of the coherent part of the electron probability density

(per unit frequency) to having its energy in the range $\hbar[\omega, \omega + d\omega]$. We note that it is possible

to integrate equation (S3) To get the explicit full electron wavefunction

$$\psi(\vec{r},t) = e^{i\left(k_0 z - \frac{U_0}{\hbar}t\right)}S(\vec{r} - vt\hat{z})e^{2i\int_0^\infty \frac{d\omega'}{\omega'}|\beta(\omega')|\sin\left(\omega'\left(t-\frac{z}{v}\right)-\arg(\beta(\omega'))\right)}. \tag{S4}$$

We thus prove the generalization of the discrete case, showing that any laser interaction
only changes the phase of the wavefunction. The resulting conservation laws for the continuous
case are discussed in the main text.

S3. Shaping attosecond electron combs: the role of the wavepacket's drift

We have shown in the main text that a drift of an electron wavepacket after a PINEM
interaction can result in temporal pulse shapes as well as in Talbot-effect patterns (generalizing

the results by the Ropers group[57]). Here we compare the resulting electron comb created by an optimized multi-harmonic laser pulse, with an electron comb created by a single frequency laser. In Fig.S2 we show the space-time drift of the two wavefunctions. Interestingly, in these plots we can see both a macro-comb of oscillations (Fig.2a,b) and inside it, a micro-comb (Fig.2c,d). We observe that each micro-comb starts with a single cycle pulse, whereas by the multi-harmonic shaping process we have this pulse appearing sooner (tens of microns instead of millimeters). Comparing the two cases, we notice that the shaping also makes the micro-comb gain a tilt and results in much narrower pulses. In Fig.S3, we present the optimal femtosecond laser pulses that were used to create the electron combs for both the single laser harmonic and multiple laser harmonics shown in Fig.S2.
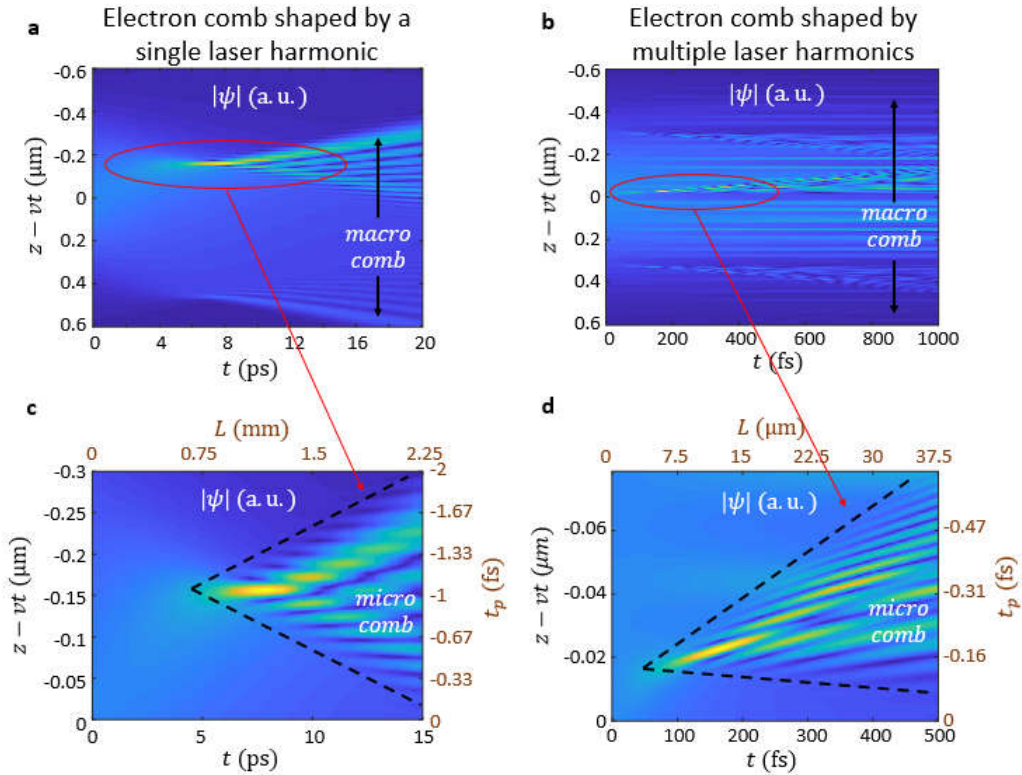
Figure S2: Wavepacket drift in the process of shaping attosecond electron combs. In all panels, we plot the space-time propagation of the wavepacket after the interaction. (a,b) Electron spatio-temporal profile resulting from a single frequency laser and an optimized laser with multiple harmonics, respectively. (c,d) Zoom-in on the micro-comb of each case in (a,b). The two horizontal axes on the top and bottom of these panels present the distance of propagation L of the pulse in parallel with the propagation time t. The two vertical axes on the right and left sides of these panels present the time t_p in the moving frame of reference in parallel with the spatial coordinate z in the frame moving with the electron velocity v.
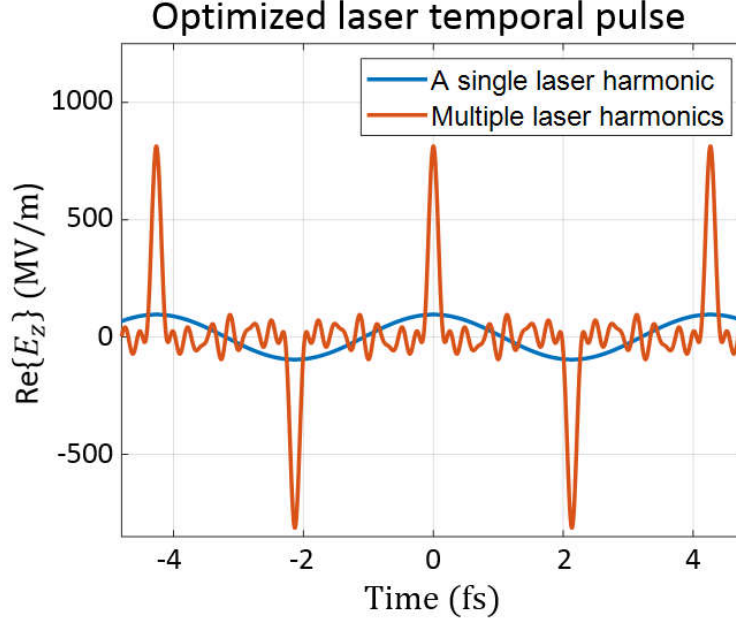
Figure S3: Temporal laser pulses for shaping attosecond electron combs. (orange) Optimal femtosecond laser pulses found by our optimization algorithm to create an electron comb, determining the initial condition ($t = 0$) wavefunctions in Fig.S2. (blue) Comparison with the temporal laser profile of a single laser harmonic. In both cases, the real part of the electric field is plotted to represent each laser pulse.

S4. Discussion of experimental realizations

The results of our paper are general for any electron-laser interaction. The geometry of the problem and the specific laser fields can always be captured by the β parameters. Nevertheless, we discuss one specific experimental realization that could implement the interaction we study, as illustrated in Fig.1 of the main text – a mirror reflecting the laser while being thin enough to remain transparent for the electrons (generalizing the paper by the Carbone group[53]).

For simplicity, we approximate the laser to be a plain wave (the electron spot size is much smaller than the laser spot size in current experiments). The electric field distribution along the z axis after reflection by a mirror with an angle θ, has the following profile:

$$E_z(z) = \begin{cases} E_0 \sin\theta e^{ik\cos\theta z} + E_0 \sin(\theta) e^{-ik\cos(\theta)z} & z < 0 \\ 0 & z > 0 \end{cases}. \tag{S5}$$

Equation (S5) neglects the contribution from the part of the field that penetrates the mirror (which was shown to be a good approximation[53]). For each laser harmonic $j\omega$, we can calculate the PINEM field according to equation (3) of the main text, resulting in

$$\beta_j(z) = \frac{ieE_0}{j\hbar\omega^2}\sin\theta\left[\frac{e^{-ij\omega\left(\frac{1}{c}\cos\theta+\frac{1}{v}\right)z}}{\frac{1}{c}\cos\theta+\frac{1}{v}} - \frac{e^{ij\omega\left(\frac{1}{c}\cos\theta-\frac{1}{v}\right)z}}{\frac{1}{c}\cos\theta-\frac{1}{v}}\right]. \tag{S6}$$

One direct consequence of equation (S6) is that as the harmonic increases, the electric field become narrower in z, and also decays more quickly. Therefore, the PINEM field decreases for larger harmonics.

We can generalize the plane wave treatment to a Gaussian laser beam analysis, and here show the scaling of the field amplitude and spatial pulse width along the z axis, being

$$E_z(\vec{r}) \propto \frac{1}{\sqrt{1+\left(\frac{2c}{w_0^2 j\omega}z\right)^2}}\exp\left(-\frac{x^2+y^2}{w_0^2\left(1+\left(\frac{2c}{w_0^2 j\omega}z\right)^2\right)}\right), \tag{S7}$$

with w_0 being a parameter that captures the laser parameters and incident angle.

In Fig.5 of the main text, we show the evolution of the electron energy spectrum along its propagation, along the interaction with the laser. Here we specify the realistic parameters that we used to show these results. As we presented in Fig.1 of the main text, we direct a laser beam at an angle α onto a mirror in order to break the uniformity of space and create a component of the electric field in the direction of the electron. Typical angles that are common in current UEM experiments include (1) laser nearly parallel to the electrons (e.g., $\alpha \approx 5°$[53]), for which we obtain short interaction lengths and high powers; (2) another accessible interaction angle has the laser nearly perpendicular to the electron (e.g., $\alpha = 85°$), which allows for long

interaction lengths but at the cost of reduced power. A typical laser waist width that matches our figure is 50 μm. These values can be easily scaled to fit all shaping scenarios we describe in the main text. To assess the feasibility of performing experiments with our techniques, we evaluate the required pulse energy to be around several nano-Joules. For example, in the case of shaping an electron comb, the required β parameters correspond to a pulse of 100 fs duration that holds an energy of ~15 nJ.